Journal of Contaminant Hydrology 187 (2016) 31–46

Contents lists available at ScienceDirect

Journal of Contaminant Hydrology

journal homepage: www.elsevier.com/locate/jconhyd

In-situ determination of field-scale NAPL mass transfer coefficients: Performance, simulation and analysis

Michael Mobile [a,b], Mark Widdowson [a,*], Lloyd Stewart [c], Jennifer Nyman [d], Rula Deeb [d], Michael Kavanaugh [d], James Mercer [e], Daniel Gallagher [a]

[a] The Charles E. Via, Jr. Department of Civil & Environmental Engineering, 750 Drillfield, Virginia Tech, Blacksburg, VA 24061-0105, USA
[b] GZA, GeoEnvironmental, Inc., Bedford, NH, USA
[c] Praxis Environmental Technologies, Inc., Burlingame, CA, USA
[d] Geosyntec Consultants, Oakland, CA, USA
[e] Tetra Tech, Sterling, VA, USA

ARTICLE INFO

Article history:
Received 13 March 2015
Received in revised form 20 January 2016
Accepted 28 January 2016
Available online 30 January 2016

Keywords:
Mass transfer
Non-aqueous phase liquid (NAPL)
Groundwater
Benzene
Petroleum hydrocarbons
Remediation

ABSTRACT

Better estimates of non-aqueous phase liquid (NAPL) mass, its persistence into the future, and the potential impact of source reduction are critical needs for determining the optimal path to clean up sites impacted by NAPLs. One impediment to constraining time estimates of source depletion is the uncertainty in the rate of mass transfer between NAPLs and groundwater. In this study, an innovative field test is demonstrated for the purpose of quantifying field-scale NAPL mass transfer coefficients (k_l^N) within a source zone of a fuel-contaminated site. Initial evaluation of the test concept using a numerical model revealed that the aqueous phase concentration response to the injection of clean groundwater within a source zone was a function of NAPL mass transfer. Under rate limited conditions, NAPL dissolution together with the injection flow rate and the radial distance to monitoring points directly controlled time of travel. Concentration responses observed in the field test were consistent with the hypothetical model results allowing field-scale NAPL mass transfer coefficients to be quantified. Site models for groundwater flow and solute transport were systematically calibrated and utilized for data analysis. Results show k_l^N for benzene varied from 0.022 to 0.60 d^{-1}. Variability in results was attributed to a highly heterogeneous horizon consisting of layered media of varying physical properties.

1. Introduction

Source zones impacted by residual non-aqueous phase liquid (NAPL) and desorbing chemicals present unique challenges for effective remediation strategies at many contaminated sites (Stroo et al., 2012; NRC, 2013). Site-specific issues impacting the efficacy of source zone remediation and the long-term persistence of NAPL sources include heterogeneous media of varying hydraulic conductivity combined with the chemical characteristics and spatial distribution of NAPL sources. Dynamic contaminant mass transfer impacted by these variables often limits the reliability of projections of remedial efficacy and source longevity (Falta et al., 2005a, 2005b; Christ et al., 2010). While analytical and semi-analytical approaches can often suffice for preliminary analyses, comprehensive models with the capacity to represent hydrogeologic and biogeochemical complexity as well as NAPL dissolution offer a more robust approach for remediation scenario testing.

Simulations of the NAPL mass transfer process are often based on either a local equilibrium or a rate-limited assumption (Zhu and Sykes, 2004), though more complex phenomenological approaches have been postulated (McCray and Dugan, 2002). The local equilibrium assumption requires thermodynamic equilibrium at the interface between the two phases (Seagren et al., 1999). In effect, mass transfer is assumed to occur instantaneously such that equilibrium is immediately

* Corresponding author.

http://dx.doi.org/10.1016/j.jconhyd.2016.01.010
0169-7722/

achieved at all locations along the contact plane. Investigators have suggested that this model may be appropriate under conditions where groundwater velocities are relatively low (Powers et al., 1992), where constituent mass fractions remain relatively significant (Powers et al., 1994b) and where contact lengths are sufficient to facilitate complete mass transfer (Geller and Hunt, 1993).

Previous studies have compared the local equilibrium and rate-limited approaches using pre-loaded, soil-packed columns (Borden and Piwoni, 1992; Seagren and Moore, 2003; Grant and Gerhard, 2007) or numerical modeling (Mayer and Miller, 1996). While these studies suggest that the local equilibrium model can perform well under certain circumstances, the results generally suggest that the rate limited approach is most appropriate at larger scales due to the potential variability in interfacial area and pore velocity (Rivett et al., 1994; Seagren et al., 1999; Grant and Gerhard, 2007; Maji and Sudicky, 2008).

The rate-limited model for NAPL mass transfer operates according to a concentration driving force multiplied by a mass transfer coefficient. Mass transfer across a plane oriented parallel to the NAPL/aqueous phase interface may be conceptualized as a Fickian analog (e.g., Seagren et al., 1999). For example, one first-order, rate-limited model takes the following form for the time-dependent mass transfer per unit volume, S_l, ($M\,L^{-3}\,T^{-1}$):

$$S_l = k_l^N (C_l^{eq} - C_l) \tag{1}$$

where C_l^{eq} is the equilibrium solubility ($M\,L^{-3}$); C_l is the instantaneous concentration of NAPL constituent l in the aqueous phase ($M\,L^{-3}$); and k_l^N is a lumped mass transfer coefficient specific to each NAPL phase constituent l (T^{-1}) (e.g., Powers et al., 1994a). Eq. (1) serves as a source term in the mass balance of aqueous phase contaminants that includes physical transport and attenuation processes. This expression accounts for a variety of influential factors including film resistance at the interface, NAPL composition and the effective solubility of each component defined according to Raoult's Law. The magnitude of the mass transfer coefficient reflects the relative degree of diffusional resistance specific to each NAPL constituent in both the NAPL and aqueous phases (Seagren et al., 1999).

Indirect techniques based on the results of column elution studies represent the majority of the literature dedicated to estimating k_l^N. Much of this work has been previously reviewed, and the authors have alluded to the general lack of detailed studies being performed at larger scales (Miller et al., 1998; Khachikian and Harmon, 2000). Many of the aforementioned column studies have resulted in the development of correlations (e.g., Gilland–Sherwood models) meant to predict k_l^N based on a set of system descriptors including compound-specific diffusivity, pore velocity and viscosity for both steady and transient conditions (Miller et al., 1990; Powers et al., 1992; Geller and Hunt, 1993; Imhoff et al., 1994; Powers et al., 1994b; Kim and Chrysikopoulos, 1999; Nambi and Powers, 2003). In most cases, the correlation-based approaches have produced reasonable results for the studied system; however, the ability to translate the models to predict mass transfer coefficients for different sets of conditions remains questionable (Abriola and Bradford, 1998; Zhu and Sykes, 2004; Grant and Gerhard, 2007). These findings are problematic as significant parameter variations with scale have been previously identified (Sale and McWhorter, 2001). Furthermore, simulated concentrations have been shown to vary significantly in studies comparing different correlations (Mayer and Miller, 1996; Zhu and Sykes, 2000; Maji and Sudicky, 2008). Thus, the applicability of Gilland–Sherwood correlations to field-scale conditions remains uncertain.

While bench-scale studies provide controlled environments under which variables contributing to k_l^N may be observed, application to field sites are prevented by heterogeneity encountered at this scale. Furthermore, complicating factors such as flow bypassing and dissolution fingering are often insignificant in laboratory column experiments but have been identified as potentially important at larger scales (Rivett and Feenstra, 2005). These issues have contributed to the need for in-situ or direct-observation techniques for determining NAPL dissolution rates at larger (i.e., field) scales. However, very few field experiments of this type have been conducted at scales larger than those encountered in bench experiments. Analysis of intermediate-scale field experiments using comprehensive models suggests that groundwater concentrations adjacent to depleting multicomponent NAPL sources are rate-limited and sensitive to NAPL mass transfer coefficients (Frind et al., 1999; Mobile et al., 2012).

At the field scale, inverse modeling of ambient monitoring data is often problematic due to resulting high parameter uncertainties and correlations (Parker et al., 2010). While this approach is common at sites with long-term historical data (i.e., plume concentrations), inverse modeling to quantify source depletion rate and NAPL mass transfer coefficients is often constrained by ineffective data resulting from unsuitable well locations and inconsistent time trends over the monitoring period. Because equilibrium conditions are typical in a source zone under an ambient hydraulic gradient and when the NAPL mass fraction of constituents of regulatory concern result in significant aqueous concentrations, perturbation of the flow field through an external stress to the system provides an opportunity to observe the response in aqueous concentration of NAPL constituents and to quantify mass transfer parameters.

Field tests of this nature have been proposed to introduce an intentional stress to the source zone flow field including push–pull tests (Istok et al., 2002; Huang et al., 2010), tracer partitioning tests (Davis et al., 2002; Dridi et al., 2009) and the Integral Pumping Test (IPT) (Bayer-Raich et al., 2006). These methods offer potential to quantify a bulk, field-scale parameter, but data developed from these methods are typically considered to be more reflective of the distribution of residual NAPL than of rate-limitations (Ptak et al., 2004). Brusseau et al. (2007) conducted an induced gradient elution test in a chlorinated solvent source zone to characterize contaminant mass transfer due to the combined effects of rate-limited sorption/desorption, diffusive mass transfer between mobile and immobile aqueous domains, and NAPL dissolution. The developing state of field techniques highlights the need for additional research directed toward evaluating mass transfer rates at larger scales.

The objective of this study is to present a field test method and data analysis technique for quantifying field-scale NAPL mass transfer coefficients. The research utilizes a newly-conceived field test (termed the Mass Transfer Test or MTT)

demonstrated in a petroleum NAPL source zone. The design of the MTT promotes rate-limited mass transfer of NAPL components such that k_l^N may be indirectly observed using aqueous phase concentration responses. As a precursor to the field demonstration of the MTT, a hypothetical numerical model was used to illustrate the approach and test sensitivity to input parameters. A description and results of the field application of the MTT will follow.

2. Overview of mass transfer test

2.1. Mass transfer test approach

The field test concept investigated here is based on the hypothesis that field-scale NAPL mass transfer rate parameters can be inversely derived if hydraulic parameters are appropriately constrained and if conditions are generated under which mass transfer is entirely rate-limited. Periods during which mass transfer displays rate-limited behavior may be isolated by observing the reaction of aqueous phase concentrations to induced hydraulic gradients or at flow velocities significant enough to overcome equilibrium maintenance where influences from external sources and sinks are limited.

Using an injection well strategically located in a contaminant source zone, a forced gradient is imposed by injecting clean water into permeable zones where residual NAPL in pore spaces or sorbed contamination along the flow path is present. Recognizing that even though determining the location and extent of a LNAPL source (i.e., light NAPL in which the specific gravity, SG < 1) is considerably less challenging than that of a DNAPL source (i.e., SG > 1), the MTT is applicable to sites where the NAPL specific gravity is both above and below unity. Similar to forced-gradient tracer tests described in Molz et al. (1988), groundwater flow for the MTT may be locally controlled either using a single injection well or by combining injection with one or more recovery wells. Monitoring wells or multi-level sampling devices are located at varying radii from the center injection well to monitor concentrations of NAPL constituents and injected tracers. Under induced flow conditions, concentrations of NAPL constituents in the aqueous phase will ultimately plateau at a level at a quasi-steady state condition (henceforth referred to as induced nonequilibrium concentrations) below their respective Raoult's Law equilibrium concentrations observed prior to the start of the MTT (i.e., initial equilibrium concentrations) when groundwater flow conditions under a natural hydraulic gradient are typical. Alternatively, a controlled shut down of groundwater extraction wells could potentially produce an increase in NAPL constituents depending on proximity and the influence of pumping to source zone monitoring wells. The test is completed when injection and pumping cease causing aqueous concentrations to rebound and plateau (henceforth referred to as final equilibrium concentration).

At sites with relatively large mass transfer coefficients, induced nonequilibrium concentrations for NAPL constituents would conceivably remain close to pre-test observations within a relatively small radius of the injection well. However, an increase in induced nonequilibrium concentrations can be expected with increased radial distance from the injection well and induced nonequilibrium concentrations decrease with greater injection rates. The transient concentration response at monitoring points observed during induced flow is then interpreted inversely using groundwater flow and solute transport modeling. The data analysis approach may depend on the level of confidence in hydrogeologic parameters (e.g., hydraulic conductivity), chemical properties of the source (e.g., NAPL composition) and data coverage. The optimized solution representing a best-fit calibration to these data provides parameter estimates for rate-limited NAPL mass transfer coefficients.

The experimental steps conducted during the MTT demonstrated in this study are summarized as follows:

1. Pre-injection monitoring
2. Clean water injection and monitoring of concentration response of NAPL constituents until induced nonequilibrium conditions are reached at monitoring wells
3. Tracer injection and monitoring of tracer concentration response at monitoring wells (optional, but recommended)
4. Post-injection monitoring.

While Steps 2 and 3 may run concurrently, each has a specific purpose and data for each are analyzed separately. Pre-injection monitoring is needed to assess initial equilibrium concentrations and initial conditions related to contaminant distribution and hydraulic gradient. In the second step water is injected into the test cell to establish a sustained, steady-state flow field for the desired rate-limited condition. A source of contaminant-free water that is compatible with the geochemistry of the aquifer is required. The concentration response (Step 2) involves sampling of monitoring wells and analysis of aqueous phase concentrations to induced gradient conditions. The tracer test is recommended for the purpose of evaluating the hydraulic conductivity field in the test cell, ideally using multi-level sampling devices. The final step involves monitoring of the rebound in NAPL constituent concentrations immediately following the conclusion of injection and extraction.

2.2. Model for data analysis

Numerical models were used for two purposes in this study: (i) to illustrate the MTT proof-of-concept through the use of a hypothetical, generic numerical model and (ii) to interpret the field test data with the objective of quantifying field-scale mass transfer coefficients for petroleum-derived NAPL constituents. Independent models were created to address both modeling objectives and to evaluate model sensitivity. Although it is conceivable that simpler analytical models could be employed for data analysis at some sites, the use of numerical models was warranted for this study due to the complexity of site hydrogeology.

Flow simulations were performed using the USGS finite-difference numerical groundwater model MODFLOW-2000 (Harbaugh et al., 2000). NAPL dissolution coupled to solute transport was simulated using the reactive transport modeling code SEAM3D (Waddill and Widdowson, 2000; Widdowson et al., 2002). SEAM3D solves the following version of the three-dimensional advection–dispersion equation which includes a NAPL-dissolution source term:

$$-\frac{\partial}{\partial x_i}(v_i C_l)+\frac{\partial}{\partial x_i}\left(D_{ij}\frac{\partial C_l}{\partial x_j}\right)+\frac{q_s}{\theta}C_l^*+k_l^N(C_l^{eq}-C_l)=R_l\frac{\partial C_l}{\partial t} \quad (2)$$

where D_{ij} is the directionally-dependent hydrodynamic dispersion coefficient tensor (L^2/T); v_i is the directionally-dependent pore velocity (L/T); q_s is the volume flow rate per unit volume of aquifer representing fluid sources and sinks (T^{-1}); C_l^* is the concentration of the external fluid source or sink flux ($M\,L^{-3}$); R_l is the dimensionless retardation factor for contaminant compound l; θ is the effective porosity; t is time; and x_{ij} is the distance along the respective Cartesian coordinate axis. Note that biodegradation is not represented in Eq. (2) but mass loss due to biotic and abiotic could be included depending on site conditions and the nature of the contaminant.

The SEAM3D NAPL dissolution (NPL) package allows for the simulation of multicomponent dissolution as represented by a spatially-dependent and temporally uniform first-order, rate-limited mass transfer according to Eq. (1). Equilibrium concentrations in the aqueous phase are predicted within the NPL package using ideal solubility, mass fraction and molecular weight information for each constituent according to Raoult's law. The NPL package calculates a mass balance on each NAPL-phase constituent which is subsequently utilized for temporally-variable equilibrium calculations. Transient NAPL constituent concentration calculations are performed using the following expression:

$$-\left(\frac{\theta}{\rho_b}\right) k_l^N \left(C_l^{eq} - C_l\right) = \frac{\partial C_l^N}{\partial t} \tag{3}$$

where C_l^N is the mass of constituent l in the local NAPL source per mass of solid (M/M) and ρ_b is the bulk density of the media (M/L^3). However, in this study the duration of the MTT did not result in any significant reduction in NAPL mass.

3. Validation: hypothetical MTT and model

A numerical model was developed and tested with the objective of evaluating the feasibility of the MTT and assessing parameter sensitivity. To accomplish this objective, a hypothetical model domain was constructed containing 10,201 active computational cells (101 rows, 101 columns). Model cell size was uniform in the horizontal direction (1.0 m by 1.0 m). A single model layer, 3 m in vertical thickness, was simulated under confined flow conditions. Specified head boundary conditions were assigned at the periphery of the model domain to maintain the confined condition and varied at periphery cells using the results of a larger flow model with a uniform initial condition for steady-state hydraulic head. Groundwater flow in the simulated test cell was driven by a single injection well and four extraction wells (Fig. 1). The spacing between the injection well and each extraction well was 31 m. Homogeneous and isotropic conditions were assumed throughout the model domain. Flow and transport input parameters used to simulate the hypothetical MTT are presented in Table 1.

3.1. Hypothetical NAPL source

The NAPL composition evaluated in this demonstration was arbitrarily constructed to reflect significant variation in mass fraction and aqueous phase solubility amongst constituents of the multicomponent NAPL mixture (Table 2). Using these chemical properties and Raoult's law, initial equilibrium concentrations for each of the four soluble NAPL constituents ranged from a maximum of 4819 mg/L for C1 to a minimum of 0.6 mg/L for C4. These values served as initial aqueous conditions for all model runs. Desorption in the source zone was assumed negligible for the hypothetical model based on the assumptions of prior equilibrium between aqueous and solid phases and NAPL dissolution significantly outweighing desorption (Johnson et al., 2003). The initial NAPL residual saturation (0.20) was set as an initial condition in every model cell as an initial condition and was sufficient to ensure no significant depletion of NAPL components during injection and to overwhelm the effect of desorption as a mass transfer mechanism. Although sorption/desorption may be a relevant mass transfer mechanism in source zones at some sites, these assumptions enabled NAPL dissolution as the primary mass transfer mechanism.

Simulated aqueous phase concentrations of the four soluble NAPL constituents were evaluated at reference cells located 4, 8 and 12 m radially from the injection well. Injection rates were tested for volumetric flow rates of 50, 100 and 200 m^3/d. Pumping rates were equally balanced amongst the four recovery wells and the cumulative total matched the injection rate. The resulting average travel velocities were 2.2, 4.4, and 8.8 m/day, respectively, at a distance of 8 m from the centroid of the cell containing the injection well. The baseline scenario NAPL mass transport coefficient ($k_l^N = 0.5\ day^{-1}$) was based in part on application of a numerical model to a depleting multicomponent NAPL (Mobile et al., 2012) and was constant for all NAPL constituents. Three alternative scenarios were tested: scenarios representing an order-of-magnitude increase and decrease (i.e., 5.0 day^{-1} and 0.05 day^{-1}, respectively) and $k_l^N = 0\ day^{-1}$ as a control simulation.

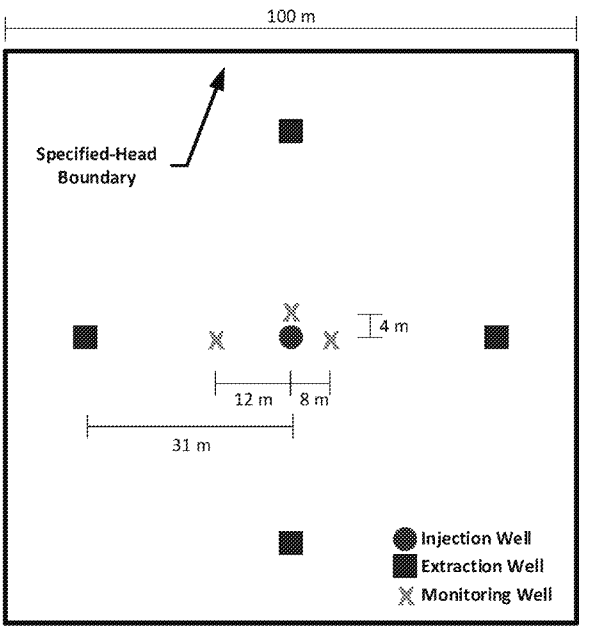

Fig. 1. Hypothetical model domain (100 m by 100 m) with variable specified hydraulic head along the periphery The flow cell consists of a single pumping well (●) in the center and four equally spaced injection wells (■) Observation wells (×) are located at radial distances of 4 m, 8 m, and 12 m from the injection well.

3.2. Hypothetical model results

Results of the hypothetical model confirm the MTT test concept; that is, the introduction of clean water into a NAPL-contaminated source zone will yield measureable changes in aqueous concentrations of NAPL constituents at nearby monitoring wells. Furthermore, the parameter k_l^N controls the degree of response in aqueous NAPL constituent concentrations and induced nonequilibrium concentrations for a given injection rate and radial monitoring distance. Simulation results show that rate-limited conditions developed at the observation point (8 m) for the most soluble component of the NAPL mixture, C1, at all tested values of k_l^N with the exception of the zero mass transfer case (Fig. 2). The limitations imposed by aqueous equilibrium are apparent prior to the passing of the flushing front for NAPL constituent C1 (<1 day). The initial constituent equilibrium concentration specified within the model implies the existence of local-equilibrium conditions; therefore, mass transfer is initially free of rate limitations and is completely governed by the lack of a concentration gradient between NAPL and aqueous phases. The subsequent transient response (1 day to approximately 3 days) reflects a period of disequilibrium during which aqueous phase flushing drives the change in simulated concentration. The rapid drop in concentration reflects the front of injected water passing through the observation point. Once flushing is complete (>3 days), a transition to rate-limitation occurs and is maintained under the induced gradient condition. As k_l^N decreased, a pronounced downward drop in concentration followed by a rapid increase to a quasi-steady state condition where an induced nonequilibrium concentration was observed. This result indicates that the impact of the advancing front of injected clean water could temporarily exceed the mass transfer of benzene at the NAPL–water interface. This finding suggests that at sites where mass transfer limitations are significant relative to the rate of injection, field observed concentrations may drop below the eventual induced nonequilibrium concentration for several days.

The sensitivity of the model to changes in k_l^N is reflected in the induced nonequilibrium concentrations developed under the final rate-limited condition (Fig. 2). Consistent with the MTT concept, the results indicate a positive correlation between the magnitude of k_l^N and the MTT-induced final equilibrium concentration for each scenario. With all other model input parameters held constant, order-of-magnitude increases and decreases in k_l^N produced percent changes in the final equilibrium concentration for C1 of +69% and −85%, respectively. Identical sensitivities were observed for the other soluble NAPL constituents (C2 through C4). The result showing that sensitivity to k_l^N is independent of composition is reasonable given that NAPL-aqueous concentration gradients are calculated as a function of a constituent-specific equilibrium and a constant NAPL mole fraction throughout the test period. However, the potential for high parameter uncertainty exists with respect to the steady concentration period because k_l^N and equilibrium concentrations are positively correlated during this period (i.e., induced nonequilibrium concentrations are sensitive to both aspects of the hypothetical system).

Results derived from extended sensitivity testing of the hypothetical model are summarized in Fig. 3 for the three most soluble NAPL constituents (C1 through C3). Steady MTT-induced concentrations at each monitoring location are plotted for the range of injection flow rates and order of magnitude variation in k_l^N. The purpose of these simulations was to identify the sensitivity of induced nonequilibrium concentration to physical parameters which may be controlled when designing and implementing a MTT. Model results were evaluated using 26 variations of the baseline scenario: $k_l^N = 0.5\ \text{day}^{-1}$, a cumulative injection/extraction rate of 100 m^3/d and a radial distance from injection of 8 m. Induced nonequilibrium concentrations were found to be more sensitive to k_l^N at shorter travel times (i.e. as pore velocities increase and travel distances decrease). This finding is highlighted in Fig. 3, where greater slopes indicate higher sensitivity to k_l^N. Slopes are greatest at the 200 m^3/d injection rate and 4 m monitoring location (upper right graph). Slopes are near 0, indicating a lack of sensitivity, for the 50 m^3/d injection rate and 12 m monitoring (lower left graph). Several of the scenarios show a steeper slope between the 0.05/d to 0.5/d k_l^Nvalues than between the 0.5/d to 5/d values. At the larger values of k_l^N, mass transfer becomes less limiting and the equilibrium concentration is less impacted.

As illustrated in Fig. 3, the likelihood for success in quantifying k_l^N is increased by using monitoring wells in relatively close proximity to the injection well and where travel time is controlled by the rate of injection per unit thickness of aquifer. Greater reductions in concentration from the initial equilibrium concentration are noted at a radial distance from injection of 4 m compared to larger travel distances. Model scenarios incorporating variations in injection rates also produced significant differences in breakthrough time which resulted in an accelerated or a delayed onset of rate-limited conditions depending on the pumping scenario. Similar results were found when testing sensitivity to radial

Table 1
Input parameters for the hypothetical groundwater flow and solute transport model.

Parameter	Value
Horizontal hydraulic conductivity (m day^{-1})	10
Effective porosity, θ (—)	0.30
Longitudinal dispersivity (m)	0.1
Horizontal transverse dispersivity (m)	0.01
Diffusion coefficient (m^2 day^{-1})	1.0×10^{-5}
Soil bulk density, ρ_b (g m^{-3})	1.5×10^6

Table 2
Baseline composition and ideal solubility of each constituent for a hypothetical NAPL consisting of four soluble compounds and an inert mass fraction. Initial concentrations were calculated using Raoult's Law.

Constituent	Mole fraction	Ideal solubility[a] (mg/L)	Initial concentration[b] (mg/L)
C1	0.482	10,000	4819
C2	0.241	1000	241
C3	0.120	100	12
C4	0.060	10	0.6
Inert	0.097	0	0

[a] Aqueous solubility of pure compound.
[b] Thermodynamic equilibrium concentration.

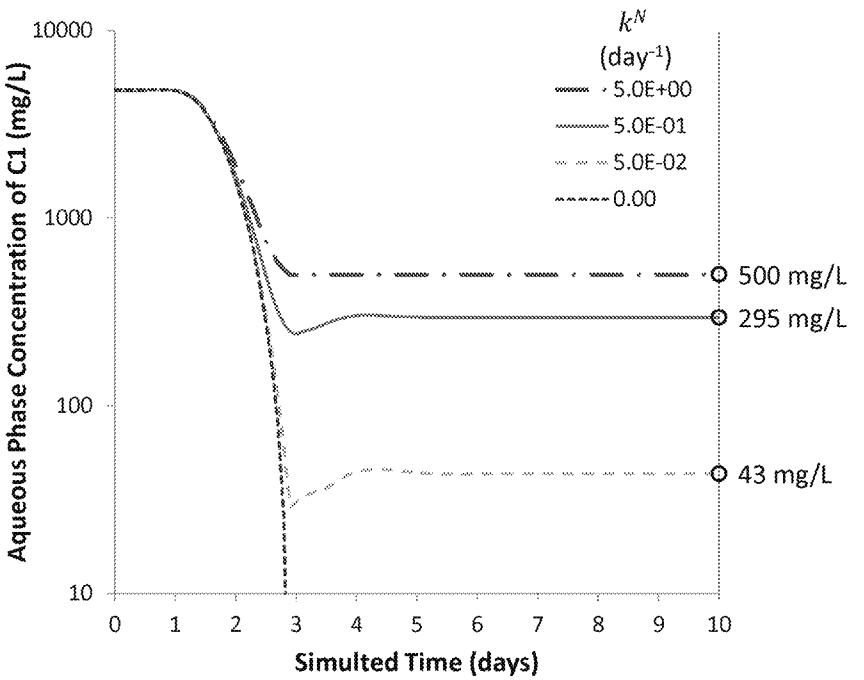

Fig. 2. Sensitivity of transient response and final induced nonequilibrium concentrations to NAPL mass transfer coefficient (k^N) using the hypothetical MTT model at a radial distance of 8 m from the injection well ($Q = 100$ m^3/d).

distance between the injection well and the observation point, as relative travel distance was found to be positively correlated with the time required to establish rate-limited conditions. These outcomes are consistent with the MTT concept and confirm the importance of consideration of aquifer hydraulic parameters in the test design.

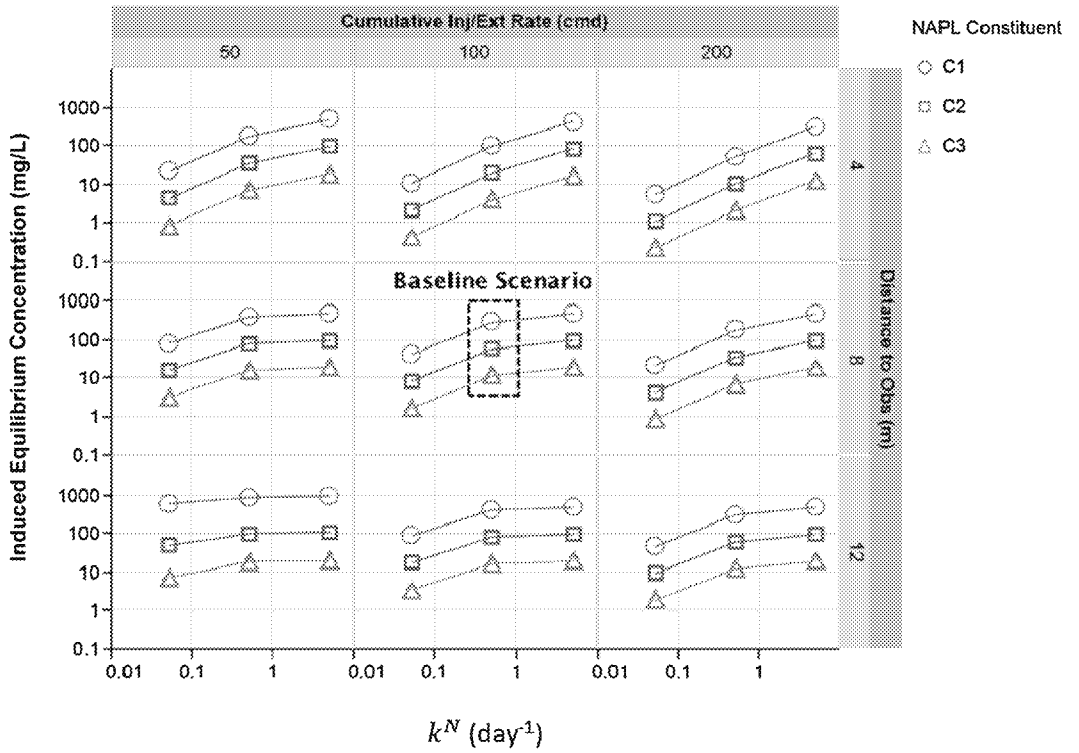

Fig. 3. Compilation of MTT-induced nonequilibrium concentration resulting from extended sensitivity simulations. Scenarios were based on variations in cumulative injection/extraction rate (m^3/d), radial distance, and the mass transfer coefficient (k^N).

4. MTT field application

A MTT field test was performed at site ST012 of the former Williams Air Force Base (WAFB) in Mesa, Arizona. ST012 served as a storage area for liquid fuels, including JP-4 and AVGAS aviation mixtures, for a significant portion of military operation at WAFB (i.e., approximately 1950 to 1990). Previous site characterization studies, occurring as early as 1984, identified significant hydrocarbon contamination in the saturated and unsaturated zones at ST012. Benzene, toluene, ethylbenzene, ortho/meta/para xylenes (e.g., BTEX) constitute the majority of the more soluble fraction of the NAPL residing in the subsurface at this site (Weidemeier et al., 1999). More recently, a pilot test was conducted to evaluate thermally enhanced extraction (TEE) to reduce the mass and longevity of the NAPL fuel source in the saturated zone (BEM Systems, 2010). The initial MTT was conducted immediately prior to the introduction of steam to the TEE test cell (Kavanaugh et al., 2011). The following sections provide an overview of the conceptual model of the site generated to guide development of a numerical model used for data analysis and quantifying mass transfer coefficients using inverse methods.

4.1. Hydrogeological setting

The lower saturated zone (LSZ) is a heterogeneous compilation of layered sands, silts and clays separated from the overlying water bearing zone by an extensive clay unit. The LSZ is segmented into two distinct permeable intervals by an additional laterally-extensive, low-permeability clay unit. The upper and lower permeable fractions of the LSZ are referred to as the B and C horizons, respectively. The B horizon is characterized by a high degree of heterogeneity resulting from coarse and fine grained sands existing with interlayered structures of low permeability silt and clay lenses. Generalized interpretations of the borehole observation data suggested preferential flow in the deeper portion of the B horizon with significant spatial variability in continuity and thickness. The C horizon is viewed as generally much less heterogeneous than the B interval and is characterized by well-sorted sands and gravels.

A rising regional water table at ST012 (approximately 1.2 m per year from 1990 through the present) has altered the LSZ from an unconfined to confined conditions. Both LSZ horizons were fully-confined in the TEE test cell area during the MTT testing period. Regional groundwater flow in the LSZ is in a west–northwest direction under ambient conditions with a hydraulic gradient of 0.005 m/m. MTT pumping and injection rates were sufficient to prevent any significant influence of ambient groundwater flow within the MTT test cell during test period. A more detailed description of the hydrogeology at ST012 is presented in BEM Systems (2010).

4.2. NAPL source zone characteristics

Prior to the mid-1990s when the water table conditions were present in the LSZ, jet fuel and aviation gasoline spilled at-or-near land surface percolated through the unsaturated zone and accumulated at the water table (Weidemeier et al., 1999). Recent site data suggest that the NAPL contamination is limited to the upper third of the C horizon but is present throughout all layers of the B horizon in the source zone (Kavanaugh et al., 2011). As water levels rose over a period of 20 years, NAPL was smeared vertically over the entire B horizon. Immediately prior to the start of the MTT, concentrations in B horizon wells ranged from 11.7 to 27.7 mg/L for benzene and 27.5 to 41.2 mg/L for BTEX. Lower concentrations were observed in C horizon wells for both benzene (0.87 to 2.29 mg/L) and BTEX (2.37 to 5.99 mg/L). These differences were attributed to compositional differences due to increased weathering and limited vertical smearing of the C horizon NAPL.

4.3. Injection/pumping scheme

The MTT at ST012 was performed by injecting clean water in the center of the test cell and extracting groundwater along a circular periphery (Fig. 4). The injection water was groundwater provided by a local utility and softened before injection to prevent mineral build-up on the well screen. Five extraction wells (LSZ-01 through LSZ-04 and LSZ-06) were oriented in a circular pattern (diameter = 43 m) with a single injection well (LSZ-07) located in the approximate center. A sixth extraction well (LSZ-05) was not operational during the MTT but was later used in the TEE pilot test. All wells were screened over the entirety of the LSZ). Extracted groundwater was treated and discharged by permit to a local municipal utility. A network of six monitoring well nests, each containing two independently-screened wells, was used for collecting concentration data during the MTT. Each well nest contained one well screened over the B horizon of the LSZ (62.8 m to 67.3 m bgs) and one well screened over the C horizon (70.0 m to 74.5 m bgs).

The initial phase of the MTT consisted of injecting water into the center well of the TEE cell to establish a steady hydraulic gradient within the test cell. Pumping of groundwater commenced simultaneously at the five extraction wells. Injection of water at LSZ-07 was maintained at a constant rate of 191 m^3/d (37 days) with the exception of a temporary shutdown that occurred 27 days from the start of injection. This period of shutdown lasted 24 days during which well pumps were replaced. Extraction rates at individual wells varied from 27 to 83 m^3/d with a combined total pumping rate of 303 m^3/d from the five pumping wells. In this field application the imbalance between the injection rate and the total rate of extraction was designed to enhance the possibility of observing induced nonequilibrium concentrations at monitoring wells located at more distant radii from the injection well.

4.4. Tracer test

A non-partitioning tracer test was conducted for the purpose of independently evaluating flow conditions within the tested region. The tracer test was initiated approximately 24 h after the start of water injection following equilibration of water levels in the LSZ test cell. A tracer mixture consisting of potassium bromide was added to the injection line over a four-hour period resulting in a bromide concentration of 2113 mg/L. Tracer breakthroughs were observed at all monitoring locations using the independent screens dedicated to the B and C horizons within the LSZ. Down-hole optical sensors (Aquistar Temphion submersible Smart pH/ISE/Redox Sensors™) recorded bromide ion concentrations and temperature using 10 min intervals following mixture injection. Sensors were placed in

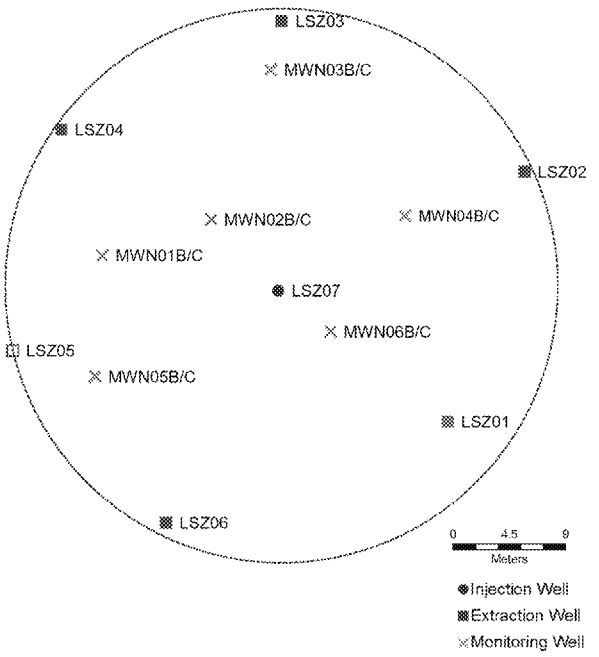

Fig. 4. Site map showing locations of center injection well, groundwater extraction wells, and monitoring well nests for the Mass Transfer Test conducted at ST012. The radius of the dashed line circle is 22.2 m from the injection well.

each monitoring and extraction well at vertical locations which corresponded to the estimated positions of the most permeable intervals within each well's screen. Kavanaugh et al. (2011) provide a more detailed discussion of the tracer tests.

4.5. TEE cell model

4.5.1. Model development

The field experiment was simulated using groundwater flow and solute transport model for the purpose of analyzing the MTT data. Similar to the approach used for the hypothetical model, groundwater flow was simulated using MODFLOW2000 (Harbaugh et al., 2000). Solute transport of BTEX compounds was simulated using SEAM3D (Waddill and Widdowson, 2000). The LSZ was discretized into a three-dimensional numerical grid with eight total model layers representing the B interval, one model layer representing the low-permeability clay separating the B and C units, and two layers representing the C interval. Layer thicknesses and material variations, shown in Fig. 5, were based on interpolated borehole log observations (BEM Systems, 2010). The numerical grid was discretized uniformly in the horizontal direction (1 m × 1 m) and consisted of an active domain containing 21,241 cells. Experimentation with non-uniform grid spacing produced no clear benefit in terms of the balance between gradient precision and computational time.

The overall process for systematic model calibration is shown in Fig. 6. Water level data collected at site-wide monitoring wells were used with a site groundwater flow model to develop boundary conditions for the MTT model. This step utilized data sets under natural groundwater flow conditions and with the injection well and pumping wells running. Tracer data were next used to calibrate the MTT groundwater flow model in conjunction with the MTT solute transport model through which layer-specific hydraulic conductivity and layer-specific effective porosity and dispersivity, respectively, were determined. Finally, the MTT transport and NAPL dissolution model was used to calibrate horizon-specific NAPL mass transfer coefficients using BTEX data collected during the MTT. Each of these steps is detailed below.

4.5.2. Groundwater boundary conditions and stresses

A site model for ST012 developed using MODFLOW2000 was employed to resolve hydraulic boundary conditions at the periphery of the TEE cell model which were assigned using a telescoping grid approach. The lateral boundaries of the model enclosed the circular pumping well network and enabled the reported extraction and injection rates to control flow conditions within the TEE cell. Transient pumping rates were simulated using the large domain/coarse grid ST012 site model, and the resulting head predictions were converted to boundary conditions for the MTT-scale model using the MODFLOW CHD package. The Multi-Node Well (MNW) package (Halford and Hanson, 2002) was used to distribute extraction and injection rates to each model layer over the span of each well screen.

4.5.3. Calibration technique — tracer simulations

Hydraulic parameters, including layer-specific hydraulic conductivity, effective porosity, and dispersivity, were evaluated using a parameter estimation process based on the breakthrough data produced from the tracer test. MT3DMS (Zheng and Wang, 1999) was used to simulate conservative solute transport emanating from the injection location. The numerical solution employs utilizes a split-operator approach in which the advective transport is solved using the total-variation-diminishing (TVD) method that is mass conservative, free of artificial oscillation and does not introduce excessive numerical dispersion (Zheng and Wang, 1999). The potassium bromide tracer pulse input at the injection wells was represented using the Source/Sink Mixing (SSM) package. Simulated concentrations were processed using the MT3DMS Transport Observation (TOB) package.

PEST (Doherty, 2005), was used to estimate the vertical distributions of hydraulic conductivity, effective porosity and longitudinal dispersivity. Model iterations tested specific sets of hydraulic parameters using MODFLOW and MT3DMS in combination with hydraulic conductivity as the controlling factor to match tracer breakthrough. At the completion of each iteration MT3DMS results were compared to tracer concentration data, and to improve the match with tracer breakthrough, hydraulic conductivity values were adjusted in MODFLOW, resulting in changes to layer-specific transmissivity and flow rates. The uniqueness of the solution was promoted by providing reasonable parameter bounds and initial estimates of based on field-test-derived hydraulic conductivity and laboratory analysis of effective porosity. Cumulative error was evaluated based on the match between observed and simulated bromide concentrations at a total of six monitoring well locations (four located in the B horizon and two located in the C horizon). Error was minimized using a least-squares approach (an iterative Gauss–Marquardt–Levenberg method of solution) based on adjustments to the hydraulic conductivity and

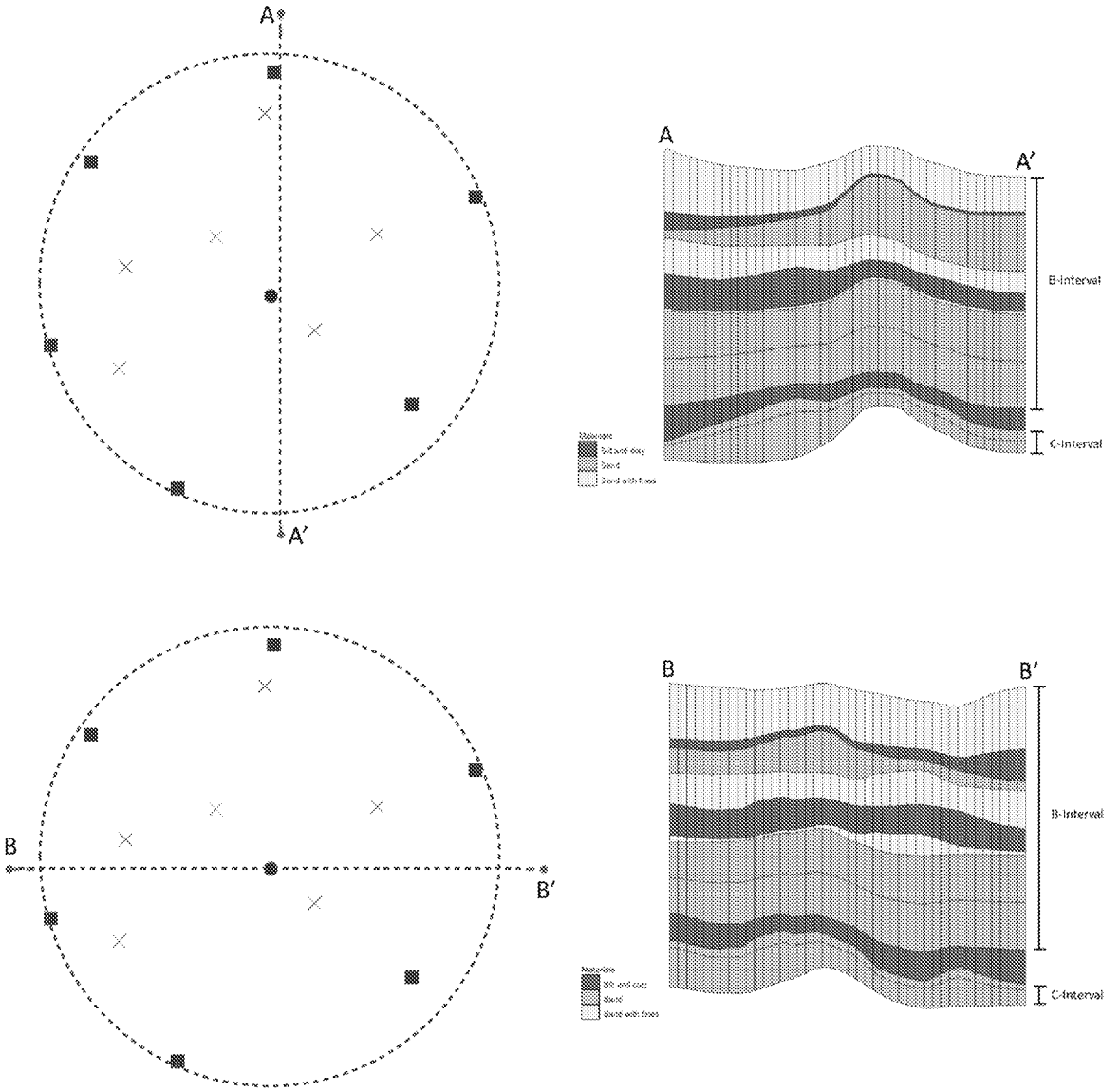

Fig. 5. Cross sections through the numerical model domain depicting hydrostratigraphy and layer thickness variations in the MTT test cell based on a solids model developed for ST012 site (BEM Systems, 2010). The radius of the dashed line circle is 22.2 m from the injection well. Average vertical thickness of the MTT test cell is 10.7 m.

refinement to the effective porosity and longitudinal dispersivity.

4.5.4. Solute transport/NAPL dissolution model

Solute transport simulations dedicated to evaluating mass transfer rate parameters were constructed from the hydrogeologic framework produced through the previously-described parameter optimization steps. Groundwater flow perturbations during the MTT were represented from the start of injection and extraction for the purpose of specifically identifying hydraulic influences on aqueous phase concentrations. The SEAM3D NPL package was modified to allow constituent-specific mass transfer coefficients for simulating mass transfer between the NAPL and aqueous phases within the TEE cell.

Model concentration variables for the MTT simulations were the individual BTEX compounds, in which xylene is the summed concentration of xylene isomers (i.e., total xylene), and an inert insoluble fraction. The initial composition of the NAPL was varied by horizon according to the maximum concentration of each NAPL constituent observed within each horizon during ambient flow periods (zero injection and extraction) prior to the MTT. This approach was consistent with the MTT conceptual model which predicts the development of initial equilibrium conditions prior to the start of injection and extraction. The BTEX mass fractions in the NAPL were specified to match compositional analysis of NAPL samples with minor

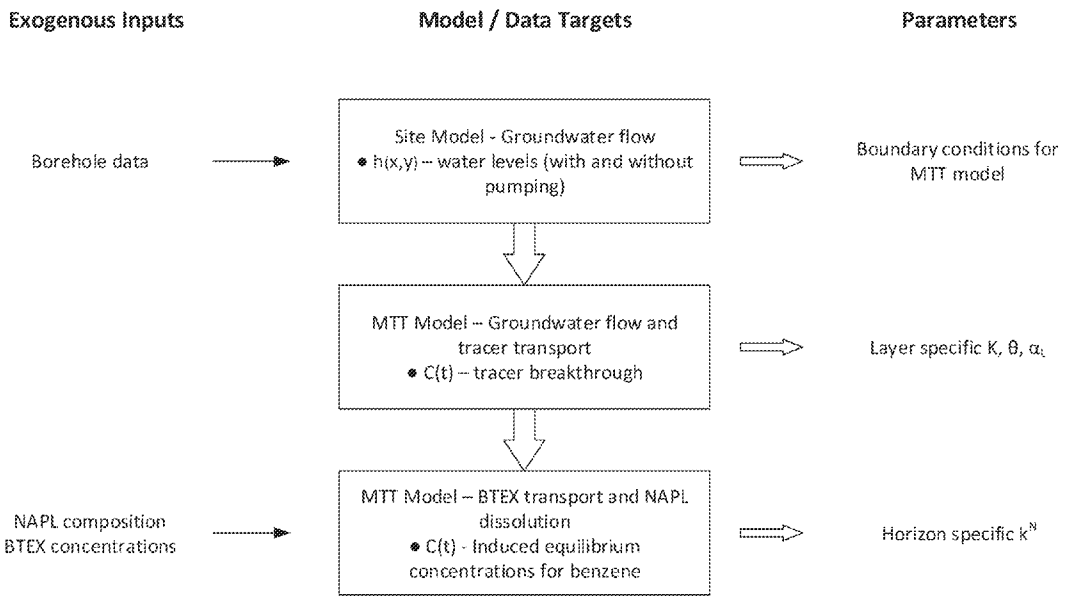

Fig. 6. Diagram illustrating the systematic procedure for model calibration used for the MTT site application to quantify NAPL mass transfer coefficients (k^N).

adjustments for consistency with the range of observed concentrations of benzene, toluene, ethylbenzene and total xylene in the source zone monitoring wells using Raoult's law, particularly in the C horizon. The remainder of the NAPL mass fraction was distributed to the inert fraction. Other NAPL constituent properties, ideal solubility and molecular weight, were assigned according to previous analyses (Kavanaugh et al., 2011). Table 3 lists the compositions used in the MTT simulations for the B and C horizons. The lower BTEX mass fractions identified in the C horizon models reflect a greater degree of weathering of the soluble fraction of the NAPL and is consistent with the trend reported at ST012 (Kavanaugh et al., 2011). Initial NAPL concentrations were assigned to reflect a residual saturation (0.10) which is consistent with significant and uniform contamination within the TEE cell and the presence of free product within the TEE cell (BEM Systems, 2010).

The SEAM3D MTT simulations were calibrated using a trial-and-error technique which focused specifically on adjusting NAPL mass transfer coefficients within the TEE cell. As noted previously and shown in Fig. 6, the only remaining input parameter for calibration of the SEAM3D model was k_l^N. Rate parameters were held constant both laterally and vertically over the volumetric regions contributing to each observation point. The mean of the observed benzene concentration data under rate-limitations (i.e., final MTT-induced nonequilibrium concentrations) served as calibration goals. Benzene data were the primary targets during the calibration process because of the high solubility of this component relative to the remaining NAPL fraction. Use of the stagnant film model (Miller et al., 1990) enabled an indirect calibration of the remaining concentration variables (i.e., TEX) by linking the NAPL mass transfer coefficients input for each constituent to the calibrated value of k_l^N for benzene. PEST-assisted inversion was impractical in this modeling phase due primarily to model complexity (i.e., calculation time required for each iteration was excessive).

4.6. Results of MTT field application

4.6.1. Hydraulic conductivity estimates

Analysis of the MTT tracer test produced parameter estimates for layer-specific hydraulic conductivity and material-specific longitudinal dispersivity and effective porosity. Hydraulic conductivity estimates over the B horizon ranged from 0.018 m/d in a silt/clay layer to a maximum value of 98 m/d in a layer of sand and gravel. Depth-averaged hydraulic conductivity for the B horizon was 24.8 m/d. In comparison, in the C horizon comprised of sand and gravel, hydraulic

Table 3
Initial NAPL compositions used in the MTT model identified by LSZ horizon. These values represent calculations based on concentration observation data collected during the MTT.

		NAPL constituent				
Parameter	Horizon	Benzene	Toluene	Ethylbenzene	Total xylenes	Inert
Mass fraction (%)	B	0.78	2	2	5.3	89.92
Mass fraction (%)	C	0.33	0.77	1.7	1.5	95.7
Ideal solubility[a] (mg/L)	B,C	1780	515	152	162	–[b]
Molecular weight (g/mol)	B,C	78.1	92.1	106	106	114

[a] Aqueous solubility of pure compound.
[b] Ideal solubility of inert fraction not required as input to the model as this parameter only influences the calculation of the equilibrium concentration in the aqueous phase.

conductivity was nearly uniform (100–102 m/d), reflecting observations of relative homogeneity noted in borehole logs. Mean values for the longitudinal dispersivity and effective porosity were 0.6 m and 0.27, respectively.

Fig. 7 shows a comparison of observed and simulated bromide breakthrough data at two monitoring wells located in the closest proximity to the injection well; one screened in the B horizon (MWN-06B) and one screened in the C horizon (MWN-02C). Observed and simulated breakthrough times, measured as the time required to half of the peak concentration, differed by 3.2 h at MWN-06B and 4.5 h at MWN-02C. While both simulations reproduced the observed breakthroughs with reasonable consistency, the slight increase in

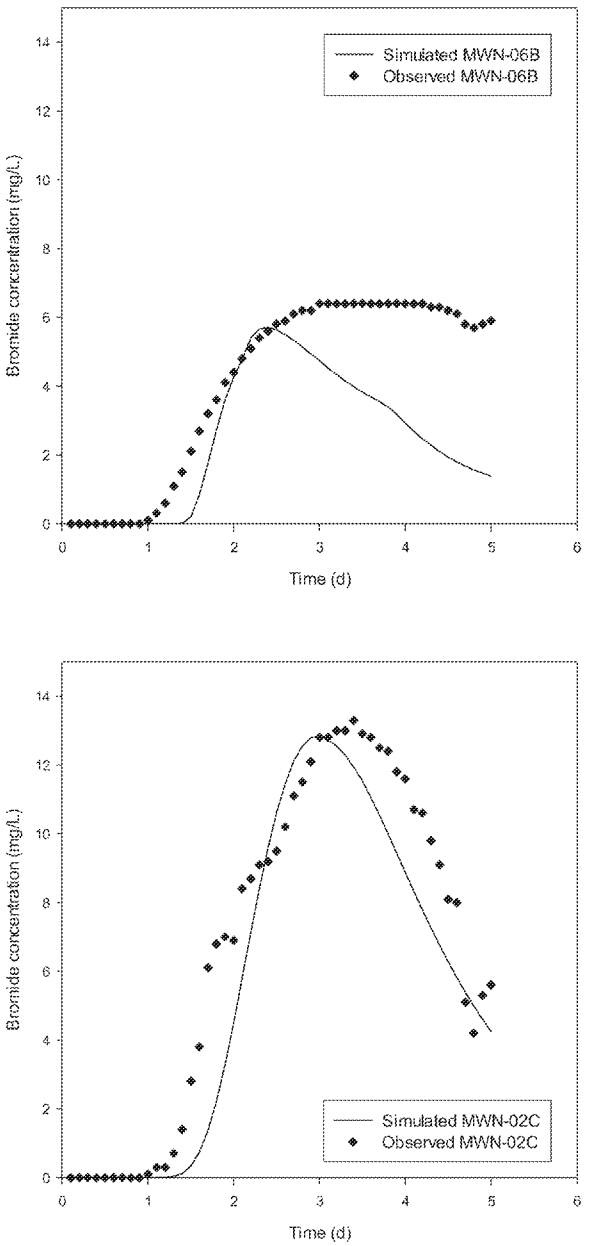

Fig. 7. Bromide tracer test results and simulations in B and C horizon monitoring wells MWN-06B (top), and MWN-02C (bottom).

error associated with the breakthrough time at MWN-02C was attributed to the greater radial distance (7.7 m) from the injection well as compared to the radial distance to MWN-06B (5.5 m). The extended plateau at MWN-06B following breakthrough is attributed to sensor malfunction over time, and specifically, oxidation of the probe membrane.

4.6.2. MTT concentration response and simulation results

Fig. 8 shows the observed benzene concentrations and best-fit simulation of the transient response following injection of water at LSZ-07 at two monitoring wells in the B horizon (MWN-02B and MWN-06B) and one well in the C horizon (MWN-06C). The observed response at the field site was consistent with the expected concentration changes based on the hypothetical model. At a radial distance of 5.5 m from the injection well (MWN-06B), the induced nonequilibrium benzene concentration represented a 96% decline relative to the observed pre-MTT initial equilibrium concentration. In comparison, a 33% decline was noted at the next nearest monitoring well (MWN-02B) at a radial distance of 7.7 m. The decline for MWN-06C was 68% and occurred more rapidly than the breakthrough at MWN-06B due to the higher hydraulic conductivity in the C horizon.

Comparisons between simulated and observed concentrations at the B and C horizon monitoring wells (Fig. 8) show the model was able to accurately reproduce transient responses without adjustment to input parameters obtained from the tracer test simulations (e.g., layer-dependent hydraulic conductivity). Simulated concentrations represent fluid flux-weighted averages calculated for each horizon. NAPL mass transfer coefficients were adjusted to calibrate the model output to the induced nonequilibrium benzene concentrations for the period immediately after injection commenced (i.e., see August 29–September 2, Fig. 8).

A validation of the model calibration was achieved using the rebound data when pumping was curtailed (Fig. 9). This condition was generated after well pumps were found to be inadequate with respect to maintaining the extraction rates required for the MTT (BEM Systems, 2010). Injection and extraction were temporarily paused to allow the pumps to be replaced; however, data collection continued within the monitoring well network. Simulation results during this period (Fig. 9, September 30–October 17) provide additional support for the calibrated value of k_l^N. The calibrated model produced a rebound consistent with the observed peak concentration at each monitoring well during the recovery period, though these observations were not explicitly considered during the model calibration process.

4.6.3. Model sensitivity

Model sensitivity to k_l^N magnitude was investigated by comparing simulations using order-of-magnitude variations in the calibrated rate parameters with the calibrated model results (Fig. 9). The results show considerable sensitivity to both an increase and decrease in k_l^N and reflect only a limited degree of spatial variability within the source zone. Increases in the calibrated values of k_l^N resulted in notable increases in induced nonequilibrium concentrations of benzene at all three observation wells. Specifically, at both MWN-02B and MWN-06C where the calibrated values of k_l^N were nearly identical, order of magnitude increases produced no change between the

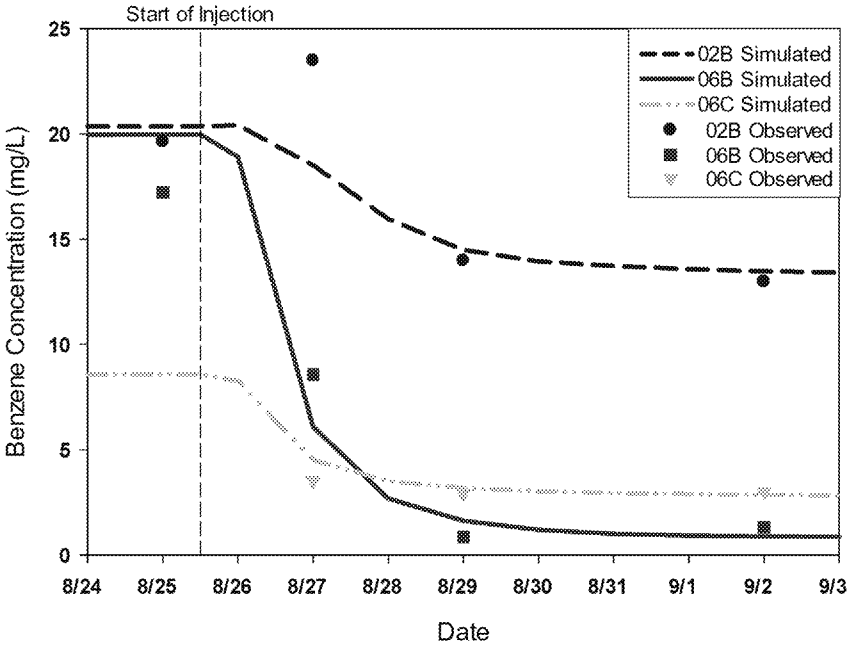

Fig. 8. Observed and simulated benzene concentrations for monitoring wells MWN-06B, MWN-02B, and MWN-06C resulting from calibrated NAPL mass transfer coefficients (0.022, 0.60, and 0.40 d^{-1} respectively).

initial and induced nonequilibrium concentrations. In this event, MTT-induced concentrations at MWN-02B and MWN-06C would remain near initial equilibrium, and thus, the local equilibrium assumption approach would be valid for this region of the source zone under this scenario.

Order of magnitude decreases in k_l^N produced a considerable decline in the induced nonequilibrium concentrations of benzene at both MWN-02B and MWN-06C. Specifically, concentration decreases of 10.7 and 2.3 mg/L, respectively, were noted. These results represent percentage decreases of 75–80% compared to the calibrated results. Simulated benzene concentrations at MWN-06B displayed less sensitivity to decreases in k_l^N (0.5 mg/L), however, this decrease represented over a 60% change relative to the induced nonequilibrium concentration shown in the calibrated model. This difference in benzene concentration is well within the range of analytical detection indicating that highly-variable NAPL mass transfer coefficients can be differentiated from MTT field data. Furthermore, the results indicate that unique solutions were obtained from analysis of the benzene concentration data and that the MTT provided reliable values of NAPL mass transfer coefficients.

4.6.4. NAPL mass transfer coefficient — calibration results

Table 4 lists the optimized values of k_l^N derived from model calibrations for each monitoring location. The results compare well to a previous study in which mean values of k_l^N for a three-component mixture of chlorinated solvents varied from 0.56 to 0.66 d^{-1} in which over an order of magnitude variation in the parameter was apparent (Mobile et al., 2012). In the B horizon, differences in the calibrated values of k_l^N between MWN-06B and MWN-02B were a direct result of differences in the induced nonequilibrium concentrations observed at the two B horizon observation wells. Although the observed response was consistent with the hypothetical model (i.e., lower induced nonequilibrium benzene concentration at MWN-06B compared to MWN-02B, approximately 1 mg/L and 13 mg/L, respectively), a larger NAPL mass transfer coefficient at MWN-02B (0.60 d^{-1}) was required to match the observed induced benzene concentration compared to the calibrated value at MWN-06B (0.022 d^{-1}).

The resulting order of magnitude difference in calibrated k_l^N values suggests that variability in field-scale NAPL mass transfer coefficients can be expected if site conditions are complex (e.g., hydrostratigraphy of the B horizon). A relevant, site-specific factor is the heterogeneous nature of the B horizon reflected in the layered material properties, as depicted in Fig. 5. Water injected into the B horizon flowed rapidly and was transported radially furthest through the sand and gravel layers, producing the greatest impact on the transient response and induced nonequilibrium concentrations at the monitoring wells. As a result, any variations in the thickness or permeability of the B horizon layers in the vicinity of the two observations are potential contributing factors in differences in the test results. In addition, variability in NAPL continuity and benzene mass fraction between layers and within layers not characterized in the field and captured in the model would also contribute to differences in k_l^N.

Comparison of simulated MTT-induced nonequilibrium concentrations with the observed data show variable correspondence for the TEX compounds (Fig. 10), but overall, the calibrated BTEX induced nonequilibrium concentrations matched the observed data reasonably well. Although k_l^N was independently calibrated at each monitoring well, the calibrated parameters were based on the benzene simulations and were not independently calibrated for each BTEX compound. Instead, calibrated k_l^N results for the TEX compounds were

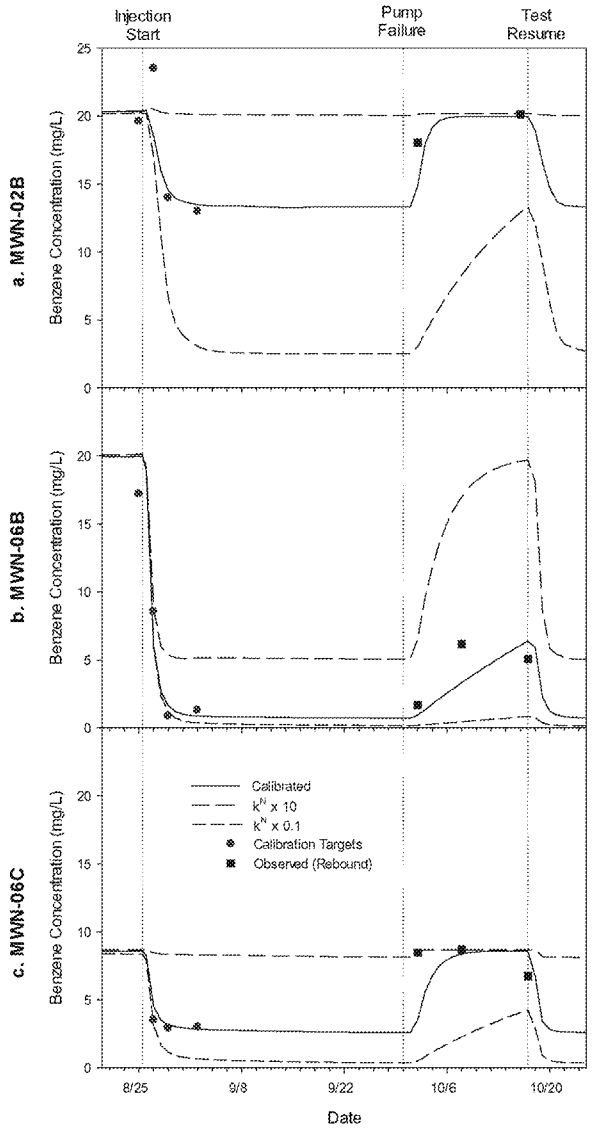

Fig. 9. Sensitivity of simulated benzene concentrations to order of magnitude variations in NAPL mass transfer coefficients at monitoring wells MWN-02B, MWN-06B, and MWN-06C. Observed concentration response to temporary stoppage in injection and extraction is denoted as rebound.

based on the ratio of the respective diffusion coefficients in water relative to benzene, an approach used for simulating dissolution of other multi-component NAPL sources (Mobile et al., 2012). Only toluene at well MWN-02B appears as an outlier, and this may reflect spatial inconsistency in benzene mass fraction relative to the TEX compounds within the B horizon. Minor spatial variations in the relatively low benzene mass fraction, which may be attributed to slight differences in weathering mechanism impacts, would explain the inconsistencies between the observed and simulated conditions. This finding is particularly meaningful as a poorly defined composition could lead to errors in k_l^N due to high parameter correlation. However, given that benzene is highly soluble and is typically the regulatory compound of concern at petroleum hydrocarbon sites, as was the case at ST012, benzene was the primary target for model simulations. At other sites with multi-component NAPL sources, it may be beneficial to independently calibrate model simulation using the full spectrum of MTT test data.

Table 4
Calibrated NAPL mass transfer coefficient for the NAPL constituents.

	Mass transfer coefficient, k_l^N (day^{-1})		
Constituent	MWN-02B	MWN-06B	MWN-06C
Benzene	0.60	0.022	0.40
Toluene	0.53	0.019	0.35
Ethylbenzene	0.48	0.018	0.32
Total xylenes	0.60	0.022	0.40

4.6.5. MTT requirements and constraints

Results of both the hypothetical study and MTT field demonstration suggest that a high quality and comprehensiveness dataset will improve the likelihood of success with model calibration and reduce uncertainty associated with the model inversion process through which k_l^N estimates are derived. Error may ultimately be the direct result of an inability to constrain hydraulic test parameters and NAPL source characteristics. Primary considerations associated with MTT design are spatial characterization of NAPL composition and initial equilibrium concentrations along with a working knowledge of NAPL distribution within the test cell.

The degree to which tracer and NAPL constituent concentration data can be vertically resolved at a test site is an important consideration in MTT design. MTT sampling strategies will be likely influenced by cost, site characteristics, and existing monitoring infrastructure. Although multi-level sampling for vertical resolution of BTEX concentrations within the B and C horizons at ST012 was technically difficult and not economically feasible, the benefit of deriving NAPL mass transfer coefficients from multi-level concentration data was demonstrated in a controlled experiment (Mobile et al., 2012). Depth-dependent k_l^N values were inversely determined by calibrating a numerical transport model to transient point concentrations collected immediately downgradient of an emplaced, multicomponent NAPL source. The calibrated model was validated through a favorable comparison of simulation results with the observed transient and cumulative flow-weighted mass discharge at extraction wells for each NAPL constituent (Mobile et al., 2012).

A number of research questions remain regarding k_l^N and its impact on NAPL source depletion time estimates. One important question is a potential decrease in the magnitude of k_l^N as the NAPL contact area for mass transfer decreases with time. While previous work has identified limited sensitivity of a NAPL volume-dependent k_l^N term on source concentration versus time in field experiments (Frind et al., 1999; Mobile et al., 2012), to the best of our knowledge this approach has not been validated over extended time frames or for highly heterogeneous, site-scale conditions. Unless considerable source zone depletion has been observed at a site, the MTT will provide data for quantifying a maximum field-scale k_l^N for the NAPL source.

A related consideration is the concern that the NAPL mass transfer coefficient quantified by an induced hydraulic gradient differs from the k_l^N under ambient groundwater flow

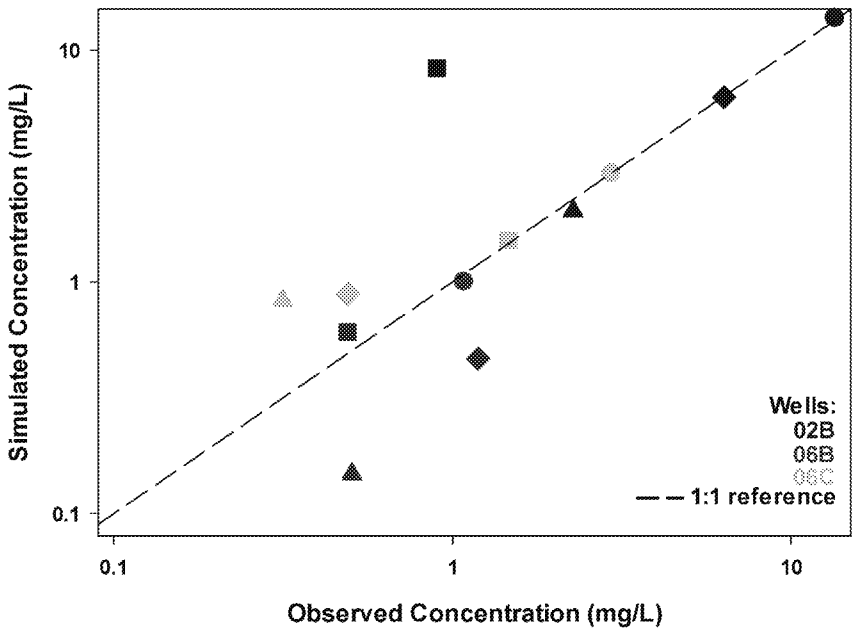

Fig. 10. Comparison of observed and simulated BTEX induced nonequilibrium concentrations at the B and C horizon monitoring wells. ● = benzene, ▲ = ethylbenzene, ■ = toluene, and ◆ = xylene.

conditions, thus limiting parameter translations to projection of source depletion. These differences are thought to stem from the phenomenological relationship between k_l^N and pore velocity documented by several studies based on the Gilland–Sherwood theory (Miller et al., 1990; Imhoff et al., 1994; Powers et al., 1994a). Nambi and Powers (2003) compared these correlations using a regression approach and showed that, while pore velocity was a statistically-significant correlation parameter, NAPL saturations alone explained the vast majority (92%) of the variation in observed Sherwood number magnitudes for a contaminated coarse sand. These findings were extended to suggest that the significance associated with the NAPL saturation term is a direct function of the degree of heterogeneity present in residual blob sizes. In the case of the ST012 MTT, the high degree of material heterogeneity combined with significant residual presence would lead to the expectation that pore velocity should have a negligible impact on predicted values of k_l^N. Extensions of the MTT approach should consider this influence, particularly when dealing with lower degrees of NAPL saturation and/or more homogeneous media. In such cases, correction factors representing scaling from induced to ambient conditions could theoretically be generated using a ratio of pore velocities between the induced and ambient conditions.

An additional level of complexity in the ST012 MTT was the multicomponent nature of the NAPL source. While not conclusive, MTT model results in this study suggest that field-scale multicomponent NAPL dissolution can be characterized as ideal according to Raoult's law if NAPL compositions are appropriately represented. The limited number of studies dedicated to multicomponent mixtures have supported ideal behavior as constrained by Raoult's law, even at larger (intermediate) scales (K. Broholm et al., 2005) and when subject to solubility enhancements (Carroll and Brusseau, 2009). However, conflicting evidence suggesting potentially non-ideal behavior has been observed in the form of non-unity activity coefficients for constituents in complex mixtures (Mukherji et al., 1997; M.M. Broholm et al., 2005). Researchers have also suggested field scale model applications to multi-component mixtures may be limited by dynamic behavior within the NAPL itself, such as uneven mixing, intra-NAPL diffusion (Khachikian and Harmon, 2000; Brahma and Harmon, 2003) and film development (Seagren et al., 1999; Ghoshal et al., 2004). In this study, the results suggest that behavioral differences in the NAPL mass transfer coefficients amongst constituents of the same NAPL were adequately explained using molecular diffusion ratios, however, minor variations in NAPL composition should not be completely dismissed as a factor.

5. Conclusions

The results of the hypothetical model and field demonstration validate the theory that rate-limited conditions can be generated using forced hydraulic gradients in NAPL-contaminated saturated groundwater systems. The hypothetical demonstration also implies that aqueous phase concentration measurements may be used to inversely estimate field-scale NAPL mass transfer coefficients governing mass transfer from multicomponent NAPL mixtures. However, as the extended sensitivity simulations suggest, consideration of MTT design variables such as injection flow rates, distance to observation wells, and the influences of hydrogeological heterogeneities are necessary in order to produce results which are valid for site-specific conditions. Fortunately, these design parameters can be evaluated before the MTT based on pumping tests and other hydrogeological data and employing pre-test models to evaluate sensitivity.

The MTT concept was successfully demonstrated in a petroleum-contaminant NAPL source zone at ST012 using

benzene as the primary NAPL constituent for evaluating NAPL mass transfer. Given the relative complexity of the B horizon and the LSZ overall, the likelihood of success at other NAPL sites is encouraging particularly where the hydrostratigraphy may be less complicated compared to ST012. In addition, the MTT concept, when properly adapted, may have application to quantifying rates of diffusion from low permeability materials in either source zones or in contaminant plumes (i.e., the back diffusion phenomenon).

The economic benefit of quantifying NAPL mass transfer coefficients by way of the MTT is difficult to project when considering that the potential value of decreased uncertainty of the long-term NAPL source depletion is not been demonstrated and has as yet been fully realized. The cost of the MTT is highly site specific but expenses may be mitigated by utilizing an existing monitoring well network. Although the MTT does not quantitatively bound an upper and lower estimate of NAPL mass or provide indirect measures of source characteristics such as pooling versus distribution as ganglia, the MTT is a step forward in field-based testing given the current constraints on estimating remediation timeframes for various source reduction scenarios.

Acknowledgements

Funding for this research was provided by the Environmental Security Technology Certification Program (ESTCP), project ER-200833, and by the Air Force Center for Environmental Excellence (AFCEE). Neither ESTCP nor AFCEE had any involvement in the collection, analysis and interpretation of data; in the writing of the report; and in the decision to submit the article for publication. The support of BEM Systems, Inc. (site contractor) is greatly appreciated.

We regret to report the passing of our co-author and colleague, Dr. James (Jim) Mercer, on March 11, 2015 after a seven-month battle with cancer. Jim was a world renowned expert in the physics, chemistry, and modeling of NAPLs in the subsurface.

References

Abriola, L.M., Bradford, S.A., 1998. Experimental investigations of the entrapment and persistence of organic liquid contaminants in the subsurface environment. Environ. Health Perspect. 106 (Supplement 4: Integrated Approaches for Studying Hazardous Substances), 1083–1095.

Bayer-Raich, M., Jarsjo, J., Liedl, R., Ptak, T., Teutsch, G., 2006. Integral pumping test analyses of linearly sorbed groundwater contaminants using multiple wells: inferring mass flows and natural attenuation rates. Water Resour. Res. 42 (8), 10.

BEM Systems, L., 2010. Phase I Thermal Enhanced Extraction (TEE) Pilot Test Performance Evaluation Report, Former Williams Air Force Base. United States Air Force, Mesa, Arizona.

Borden, R.C., Piwoni, M.E., 1992. Hydrocarbon dissolution and transport: a comparison of equilibrium and kinetic models. J. Contam. Hydrol. 10, 309–323.

Brahma, P.P., Harmon, T.C., 2003. The effect of multicomponent diffusion on NAPL dissolution from spherical ternary mixtures. J. Contam. Hydrol. 67 (1–4), 43–60.

Broholm, K., Feenstra, S., Cherry, J.A., 2005a. Solvent release into a sandy aquifer. 2. Estimation of DNAPL mass based on a multiple-component dissolution model. Environ. Sci. Technol. 39 (1), 317–324.

Broholm, M.M., Christophersen, M., Maier, U., Stenby, E.H., Höhener, P., Kjeldsen, P., 2005b. Compositional evolution of the emplaced fuel source in the vadose zone field experiment at airbase Vaerlose, Denmark. Environ. Sci. Technol. 39 (21), 8251–8263.

Brusseau, M.L., et al., 2007. Source-zone characterization of a chlorinated-solvent contaminated superfund site in Tucson, AZ. J. Contam. Hydrol. 90 (1–2), 21–40.

Carroll, K.C., Brusseau, M.L., 2009. Dissolution, cyclodextrin-enhanced solubilization, and mass removal of an ideal multicomponent organic liquid. J. Contam. Hydrol. 106 (1–2), 62–72.

Christ, J.A., Ramsburg, C.A., Pennell, K.D., Abriola, L.M., 2010. Predicting DNAPL mass discharge from pool-dominated source zones. J. Contam. Hydrol. 114 (1–4), 18–34.

Davis, B.M., Istok, J.D., Semprini, L., 2002. Push–pull partitioning tracer tests using radon-222 to quantify non-aqueous phase liquid contamination. J. Contam. Hydrol. 58 (1–2), 129–146.

Doherty, J., 2005. PEST: Model-Independent Parameter Estimation.

Dridi, L., Pollet, I., Razakarisoa, O., Schafer, G., 2009. Characterisation of a DNAPL source zone in a porous aquifer using the partitioning interwell tracer test and an inverse modelling approach. J. Contam. Hydrol. 107 (1–2), 22–44.

Falta, R.W., Basu, N., Rao, P.S., 2005a. Assessing impacts of partial mass depletion in DNAPL source zones: II. Coupling source strength functions to plume evolution. J. Contam. Hydrol. 79 (1–2), 45–66.

Falta, R.W., Rao, P.S., Basu, N., 2005b. Assessing the impacts of partial mass depletion in DNAPL source zones – I. Analytical modeling of source strength functions and plume response. J. Contam. Hydrol. 78 (4), 259–280.

Frind, E.O., Molson, J.W., Schirmer, M., Guiguer, N., 1999. Dissolution and mass transfer of multiple organics under field conditions: the Borden emplaced source. Water Resour. Res. 35 (3), 683–694.

Geller, J.T., Hunt, J.R., 1993. Mass-transfer from nonaqueous phase organic liquids in water-saturated porous-media. Water Resour. Res. 29 (4), 833–845.

Ghoshal, S., Pasion, C., Alshafie, M., 2004. Reduction of benzene and naphthalene mass transfer from crude oils by aging-induced interfacial films. Environ. Sci. Technol. 38 (7), 2102–2110.

Grant, G.P., Gerhard, J.I., 2007. Simulating the dissolution of a complex dense nonaqueous phase liquid source zone: 2. Experimental validation of an interfacial area - based mass transfer model. Water Resour. Res. 43 (12), 18.

Halford, K.J., Hanson, R.T., 2002. User Guide for the Drawdown-Limited, Multi-Node Well (MNW) Package for the U.S. Geological Survey's Modular Three-Dimensional Finite-Difference Ground-Water Flow Model, Versions MODFLOW-96 and MODFLOW-2000. U.S. Geological Survey, Sacramento, California.

Harbaugh, A.W., Banta, E.R., Hill, M.C., McDonald, M.G., 2000. MODFLOW-2000, the U.S. Geological Survey Modular Ground-Water Model – User Guide to Modularization Concepts and the Ground-Water Flow Process.

Huang, J.Q., Christ, J.A., Goltz, M.N., 2010. Analytical solutions for efficient interpretation of single-well push–pull tracer tests. Water Resour. Res. 46.

Imhoff, P.T., Jaffe, P.R., Pinder, G.F., 1994. An experimental study of complete dissolution of a nonaqueous phase liquid in saturated porous media. Water Resour. Res. 30 (2), 307–320.

Istok, J.D., Field, J.A., Schroth, M.H., Davis, B.M., Dwarakanath, V., 2002. Single-well "push–pull" partitioning tracer test for NAPL detection in the subsurface. Environ. Sci. Technol. 36 (12), 2708–2716.

Johnson, G.R., Zhang, Z., Brusseau, M.L., 2003. Characterizing and quantifying the impact of immiscible-liquid dissolution and nonlinear, rate-limited sorption/desorption on low-concentration elution tailing. Water Resour. Res. 39 (5), 8.

Kavanaugh, M.C., Deeb, R., Nyman, J., Stewart, L., Widdowson, M., 2011. Improved Field Evaluation of NAPL Dissolution and Source Longevity. ESTCP, Arlington, VA.

Khachikian, C., Harmon, T.C., 2000. Nonaqueous phase liquid dissolution in porous media: current state of knowledge and research needs. Transp. Porous Media 38 (1–2), 3–28.

Kim, T.J., Chrysikopoulos, C.V., 1999. Mass transfer correlations for nonaqueous phase liquid pool dissolution in saturated porous media. Water Resour. Res. 35 (2), 449–459.

Maji, R., Sudicky, E.A., 2008. Influence of mass transfer characteristics for DNAPL source depletion and contaminant flux in a highly characterized glaciofluvial aquifer. J. Contam. Hydrol. 102 (1–2), 105–119.

Mayer, A.S., Miller, C.T., 1996. The influence of mass transfer characteristics and porous media heterogeneity on nonaqueous phase dissolution. Water Resour. Res. 32 (6), 1551–1567.

McCray, J.E., Dugan, P.J., 2002. Nonideal equilibrium dissolution of trichloroethene from a decane-based nonaqueous phase liquid mixture: experimental and modeling investigation. Water Resour. Res. 38 (7), 1097.

Miller, C.T., Poirier-McNeill, M.M., Mayer, A.S., 1990. Dissolution of trapped nonaqueous phase liquids: mass-transfer characteristics. Water Resour. Res. 26 (11), 2783–2796.

Miller, C.T., Christakos, G., Imhoff, P.T., McBride, J.F., Pedit, J.A., Trangenstein, J.A., 1998. Multiphase flow and transport modeling in heterogeneous porous media: challenges and approaches. Adv. Water Resour. 21 (2), 77–120.

Mobile, M.A., Widdowson, M.A., Gallagher, D.L., 2012. Multicomponent NAPL source dissolution: evaluation of mass-transfer coefficients. Environ. Sci. Technol. 46 (18), 10047–10054.

Molz, F.J., Güven, O., Melville, J.G., Nohrstedt, J.S., Overholtzer, J.K., 1988. Forced-gradient tracer tests and inferred hydraulic conductivity distributions at the mobile site. Ground Water 26 (5), 570–579.

Mukherji, S., Peters, C.A., Weber, W.J., 1997. Mass transfer of polynuclear aromatic hydrocarbons from complex DNAPL mixtures. Environ. Sci. Technol. 31 (2), 416–423.

Nambi, I.M., Powers, S.E., 2003. Mass transfer correlations for nonaqueous phase liquid dissolution from regions with high initial saturations. Water Resour. Res. 39 (2), 11.

National Research Council (NRC), 2013. Alternatives for Managing the Nation's Complex Contaminated Groundwater Sites. National Academies Press, Washington, DC.

Parker, J.C., Kim, E., Widdowson, M., Kitanidis, P., Gentry, P., 2010. Effects of model formulation and calibration data on uncertainty in predictions of DNAPL source dissolution rate. Water Resour. Res. 46, W12517. http://dx.doi.org/10.1029/2010WR009361.

Powers, S.E., Abriola, L.M., Weber, W.J., 1992. An experimental investigation of nonaqueous phase liquid dissolution in saturated subsurface systems: steady-state mass-transfer rates. Water Resour. Res. 28 (10), 2691–2705.

Powers, S.E., Abriola, L.M., Dunkin, J.S., Weber, W.J., 1994a. Phenomenological models for transient NAPL-water mass-transfer processes. J. Contam. Hydrol. 16 (1), 1–33.

Powers, S.E., Abriola, L.M., Weber, W.J., 1994b. An experimental investigation of nonaqueous phase liquid dissolution in saturated subsurface systems: transient mass-transfer rates. Water Resour. Res. 30 (2), 321–332.

Ptak, T., Piepenbrink, M., Martac, E., 2004. Tracer tests for the investigation of heterogeneous porous media and stochastic modelling of flow and transport — a review of some recent developments. J. Hydrol. 294 (1–3), 122–163.

Rivett, M.O., Feenstra, S., 2005. Dissolution of an emplaced source of DNAPL in a natural aquifer setting. Environ. Sci. Technol. 39 (2), 447–455.

Rivett, M.O., Feenstra, S., Cherry, J.A., 1994. Transport of a dissolved-phase plume from a residual solvent source in a sand aquifer. J. Hydrol. 159 (1–4), 27–41.

Sale, T.C., McWhorter, D.B., 2001. Steady state mass transfer from single-component dense nonaqueous phase liquids in uniform flow fields. Water Resour. Res. 37 (2), 393–404.

Seagren, E.A., Moore, T.O., 2003. Nonaqueous phase liquid pool dissolution as a function of average pore water velocity. J. Environ. Eng. ASCE 129 (9), 786–799.

Seagren, E.A., Rittmann, B.E., Valocchi, A.J., 1999. A critical evaluation of the local-equilibrium assumption in modeling NAPL-pool dissolution. J. Contam. Hydrol. 39 (1–2), 109–135.

Stroo, H.F., Leeson, A., Marqusee, J.A., Johnson, P.C., Ward, C.H., Kavanaugh, M.C., Sale, T.C., Newell, C.J., Pennell, K.D., Lebrón, C.A., Unger, M., 2012. Environ. Sci. Technol. 46 (12), 6438–6447.

Waddill, D.W., Widdowson, M.A., 2000. SEAM3D: a numerical model for three-dimensional solute transport and sequential electron acceptor-based bioremediation in groundwater. ERDC/EL TR-00-X. U.S. Army Engineer Research and Development Center, Vicksburg, MS (89 pp.).

Weidemeier, T.H., Rifai, H.S., Newell, C.J., Wilson, J.T., 1999. Natural Attenuation of Fuels and Chlorinated Solvents in the Subsurface. John Wiley and Sons, NY, NY (617 pp.).

Widdowson, M.A., Waddill, D.W., Brauner, J.S., Chapelle, F.H., 2002. SEAM3D: A Numerical Model for Three-Dimensional Solute Transport Coupled to Sequential Electron Acceptor-Based Biological Reactions in Groundwater. Virginia Polytechnic Institute and State University, Blacksburg, VA.

Zheng, C., Wang, P.P., 1999. MT3DMS: A Modular Three-Dimensional Multispecies Transport Model for Simulation of Advection, Dispersion, and Chemical Reactions of Contaminants in Groundwater Systems; Documentation and User's Guide (prepared for U.S. Army Crops of Engineers).

Zhu, J., Sykes, J.F., 2000. The influence of NAPL dissolution characteristics on field-scale contaminant transport in subsurface. J. Contam. Hydrol. 41 (1–2), 133–154.

Zhu, J.T., Sykes, J.F., 2004. Simple screening models of NAPL dissolution in the subsurface. J. Contam. Hydrol. 72 (1–4), 245–258.